Green Chemistry

Accepted Manuscript

ROYAL SOCIETY OF CHEMISTRY

www.rsc.org/greenchem

Beyond Biocompatibility: A Novel Approach for the Synthesis of ZnS Quantum Dot-Chitosan Nano-Immunoconjugates for Cancer Diagnosis

Herman S. Mansur[1*], Alexandra A. P. Mansur[1], Amanda Soriano-Araújo[1], Zélia I. P. Lobato[2]

[1]Center of Nanoscience, Nanotechnology, and Innovation - CeNano[2]I, Department of Metallurgical and Materials Engineering, Federal University of Minas Gerais, Brazil;

[2]Department of Preventive Veterinary Medicine, Veterinary School, Federal University of Minas Gerais, Brazil

ABSTRACT

In this study, we designed and developed novel biocompatible ZnS quantum dot (QD) nano-immunoconjugates to detect cancer cells strictly *via* an environmentally-friendly chemistry process. ZnS QDs were capped by chitosan-based ligands that were chemically conjugated at room temperature with an antibody-specific cancer biomarker for non-Hodgkin lymphoma using a one-pot aqueous colloidal route. The nano-immunoconjugates were extensively characterised by several spectroscopic and morphological approaches and biological assays. The results demonstrated that ultra-small colloidal ZnS nanocrystals with average diameters of 3.7 nm were produced and stabilised by the chitosan-antibody conjugates. In addition, they exhibited intense fluorescence activity and were effective for specific targeting, labelling, and bioimaging of cancerous lymphocyte B-cells. Moreover, the results of *in vitro* cell viability assays using fibroblast cell line indicated that the ZnS-nanoconjugates were cytocompatible. These may be used in numerous applications in oncology diagnosis and nanomedicine.

Keywords: Nanoparticles; Nanomedicine; Water-soluble colloids; Sustainable Nanomaterials; Nanobioconjugates.

[*] To whom correspondence should be addressed: Federal University of Minas Gerais, Av. Antônio Carlos, 6627 – Escola de Engenharia, Bloco 2 – Sala 2233, 31.270-901, Belo Horizonte/MG, Brazil; Tel: +55-31-34091843; Fax: +55-31-34091815; E-mail: hmansur@demet.ufmg.br (H. Mansur)

1. INTRODUCTION

In the last few decades, the use of nanotechnology in the biological, pharmaceutical, and health sciences has significantly increased, leading to noteworthy improvements in life expectancies worldwide [1-9]. Nonetheless, a major effort is required to overcome major challenges, such as increasing the human life span and improving the quality of life. Thus, nanomedicine has emerged as an innately multidisciplinary field combining aspects of nanotechnology, biology, and medicine. In the field of oncology with millions of fatalities and new cases every year, nanomedicine is expected to play a critical and definitive role owing to its ground-breaking diagnostic tools for the earliest possible detection of primary cancers and advanced therapeutic methods for effectively and selectively killing tumour cells [8-11]. The most promising aspect of nanoscale-designed materials in oncology rests in their potential for bio-functionalisation for targeted therapy, thus, minimizing or even eliminating the common, severe collateral effects of chemotherapeutics [3,4,8-11].

Currently, several nanoscale materials, such as semiconductor nanoparticles (i.e., quantum dots, QDs), may be utilized to produce novel nanostructures and nanoconjugates for biomedical applications owing to their remarkable electronic, optical, and magnetic properties [12-14]. QDs have been used as luminescent probes in the fields of biology, medicine, and pharmacy as they offer a brighter and narrower emission and a higher signal to noise ratio compared with conventional organic dyes [9-12,15]. However, to date, most QDs are synthesised using traditional organometallic methods with organic solvents at high temperatures, with the inorganic semiconductor core usually made of toxic elements (Cd^{2+}, Pb^{2+}), and stabilised by organic ligands (e.g. triocytlphosphine, TOP and triocytlphosphine oxide, TOPO) harmful to the eco-system [12,16-17]. Even so, cadmium-based QDs (chalcogenides) have been largely developed for biomedical applications as they can be passivated by another semiconductor 'shell' (heterostructure) and also surrounded by biocompatible and non-toxic ligands, such as polymers, amino acids, proteins, and carbohydrates [12,18-21]. Theoretically, this strategy would shield and ultimately eliminate the harmful release of toxic metal cations of the QDs under biological and environmental applications, as reported in an elegant paper published based on a pilot study in non-human primates [17]. However, it is still controversial the use of QDs with Cd-based cores as nanoprobes for nanomedicine and eco-friendly applications, because their long-term impact is not fully understood yet [17]. Thus, it is important to develop processes for the production of non-toxic QDs with the desired optical and chemical properties in a biocompatible and environmentally-friendly manner. Although, there are some interesting reviews on the themes of nanomedicine and sustainable chemistry [22-24] and some uncommon efforts to develop greener synthetic methods for QD-nanomaterials [25-27], no reports in the consulted literature have addressed nanoscience and nanotechnology strategies for the diagnosis, imaging, and therapy of cancer using biocompatible water-soluble QDs and eco-

friendly chemical processes. Hence, cadmium-free quantum dots, such as those based on zinc chalcogenides (ZnSe, ZnS) and Zn-doped semiconductor compounds (e.g. Mn^{2+}, Fe^{3+}, Cu^{+}, Ni^{2+}) [5,28], offer very promising alternatives for producing non-toxic and environmentally-friendly nanomaterials. In addition, the possibility of producing hybrid nanoconjugates is attractive because these materials may combine the intrinsic functionalities of inorganic nanoparticles and the biointerfaces presented by biomolecules and polymers of natural origin, such as carbohydrates, glycoconjugates, enzymes, proteins, and DNA [3-5,7,11]. In this sense, chitosan (poly-β(1→4)-2-amino-2-deoxy-D-glucose) and its derivatives are commonly preferred as carbohydrate-based components for developing medical, pharmaceutical, and nutrition applications, owing to their non-toxicity, biocompatibility, physico-chemical and mechanical properties, and relative chemical solubility and stability in aqueous medium and the environment [5-7,11]. Moreover, chitosan is an abundant, eco-friendly and commercially available biopolymer. Considering an environmentally-friendly chemistry approach, it is of paramount importance to produce nanomaterials and nanoconjugates at low temperatures that are not harmful to human health or the environment, minimizing or eliminating toxic ingredients in the process, using natural renewable sources wherever possible in all stages, ranging from the design to the engineering of systems [19, 29].

Thus, we endeavoured to develop a sustainable synthesis of fluorescent ZnS QDs capped with chitosan-antibody immunoconjugates using a facile, reproducible, and economical one-pot aqueous processing method at room temperature. Moreover, these fluorescent ZnS nanoconjugates were cytocompatible and effective for specific targeting, labelling, and bioimaging of cancerous lymphocyte B-cells.

2. EXPERIMENTAL PROCEDURE

2.1. Materials

Zinc chloride ($ZnCl_2$, ≥ 98%; Sigma-Aldrich, USA), sodium sulphide ($Na_2S{\cdot}9H_2O$, >98%; Synth, Brazil), sodium hydroxide (NaOH, ≥99%; Merck, USA), acetic acid (CH_3COOH, ≥99.7%; Synth, Brazil), hydrochloric acid (HCl, 36.5–38.0%; Sigma-Aldrich, USA), 1-ethyl-3-[3-dimethylaminopropyl]carbodiimide hydrochloride (EDC, $C_8H_{17}N_3{\cdot}HCl$, ≥98%; Sigma, USA), and N-hydroxysulfosuccinimide sodium salt (sulfo-NHS, $C_4H_4NNaO_6S$, ≥98%; Aldrich, USA) were used as received. Low molecular weight chitosan powder (catalogue #448869, M_W = 60–70 kDa; degree of deacetylation [DD] = 96.1%; viscosity = 35 cPoise, 1 wt. % in 1% acetic acid; Aldrich Chemical, USA) was used as a reference polysaccharide ligand. An anti-CD20 polyclonal antibody (abCD20) was supplied by Abcam (Cambridge, MA, USA). Unless indicated otherwise, deionised water (DI water, Millipore Simplicity™) with a resistivity of 18

MΩ·cm was used to prepare solutions, and procedures were conducted at room temperature (RT, 23 ± 2ºC).

2.2. Synthesis of ZnS QDs immunoconjugates

A chitosan acetate solution (1%, w/v) was prepared by adding chitosan powder (0.5 g) to a 50 mL aqueous solution (2%, v/v) of acetic acid and stirring overnight at room temperature until complete solubilisation occurred (pH ~3.6). The pH value of the chitosan acetate solution was adjusted to 6.0 ± 0.1 with NaOH (0.1 $mol \cdot L^{-1}$), resulting in a sodium acetate-buffered solution, referred to here as 'CHI'. $ZnCl_2$ (8.0×10^{-3} $mol \cdot L^{-1}$), $Na_2S \cdot 9H_2O$ (1.0×10^{-2} $mol \cdot L^{-1}$), EDC (1.0 wt. %), and sulfo-NHS (2.5 wt. %) solutions were prepared in deionised water. An anti-CD20 polyclonal antibody (abCD20) was used as received (0.9 $mg \cdot mL^{-1}$).

ZnS QD immunoconjugates ("ZnS_CHI-abCD20") were synthesised *via* an aqueous route at room temperature (RT) in a reaction flask as follows. Briefly, 0.4 $mg \cdot mL^{-1}$ of CHI in DI water was added to a flask. Next, Zn^{2+} ($ZnCl_2$, 0.75 $mmol \cdot L^{-1}$) and S^{2-} ($Na_2S \cdot 9H_2O$, 0.37 $mmol \cdot L^{-1}$) precursor solutions were added to the flask, with moderate magnetic stirring for 10 min. The S:Zn molar ratio was 1:2. Under continuous stirring, an abCD20 antibody (3.0 $\mu g \cdot mL^{-1}$, pre-mixed for 15 min at 6 ± 2ºC with a 0.24 $mmol \cdot L^{-1}$ EDC solution) and sulfo-NHS solution (0.70 $mmol \cdot L^{-1}$) were introduced into the flask, and the system was incubated at 6 ± 2ºC overnight. As a reference, a sampling aliquot of the suspension (referred to as 'ZnS_CHI') was collected before antibody addition. The ZnS QD colloids were purified against excess of DI water for 48h at 6±2 ºC under magnetic stirring using dialysis membranes (Pur-A-Lyzer™ Mega dialysis kit, Sigma) with cut-off molecular weight of 12,000-14,000 Da.

2.3. Characterisation of ZnS QDs immunoconjugates

Antibody-chitosan conjugation was evaluated by sodium dodecyl sulphate-polyacrylamide gel electrophoresis analysis (SDS-PAGE) and Fourier transform infrared (FTIR) spectroscopy. Antibodies (abCD20) and immunoconjugates were analysed by electrophoresis on precast 4–12% gradient polyacrylamide SDS gels (Amersham ECL Gels; GE Healthcare, Uppsala, Sweden). Gels were stained with Coomassie Brilliant Blue R-250 to identify the antibody. QD suspensions were also analysed by the transmission (direct) FTIR spectroscopy method, using a Nicolet iN10 infrared microscope (Thermo Scientific) over the range of 4000 to 400 cm^{-1}, with 64 scans and a resolution of 4 cm^{-1}. Samples were prepared by placing a droplet of the suspension on KBr powder, drying for 24 h at 60 ± 2ºC, and then pressing the powder into a transmission pellet.

UV-Visible (UV-Vis) spectroscopy measurements were conducted by placing samples in a quartz cuvette and taking spectral measurements in a Lambda EZ-210 spectrophotometer (Perkin-Elmer) in transmission mode, over a wavelength range of 600 nm to 190 nm. All

experiments were conducted in triplicates (n = 3) unless specifically noted and data were presented as mean ± standard deviation.

Zeta potential (ZP) and Dynamic Light Scattering (DLS) analyses were performed using a Brookhaven ZetaPALS instrument with a laser wavelength of 660 nm (35 mW, red diode laser). Standard square acrylic cells with a volume of 4.5 mL were used. ZP measurements were performed at (25.0 ± 2ºC) under the Smoluchowski approximation [30]. For DLS measurements of QDs, the colloidal solutions were filtered 4 times through a 0.45-µm aqueous syringe filter (Millex LCR 25 mm, Millipore) to remove any potential dust particles. Samples were measured at 25 ± 2ºC, and light scattering was detected at 90º.

Photoluminescence (PL) characterisation of ZnS immunoconjugates was conducted based on spectra acquired at room temperature using a high power xenon light source (HPX-2000, Mikropack) coupled to an Ocean Optics USB2000 UV-VIS spectrophotometer. All tests were performed using a minimum of 4 repetitions ($n \geq 4$). Additionally, QD colloidal media were placed inside a "darkroom-chamber" where they were illuminated by a UV radiation emission bulb ($\lambda_{excitation}$ = 365 nm, 6 W, Boitton Instruments). Digital colour images were collected of the fluorescence of the QDs in the visible range of the spectrum. QD colloidal media were also dropped onto glass slides and the fluorescence responses were characterised with a Ti-U inverted fluorescence microscope (Nikon; 130 W/Hg lamp, 10× objective, 10× eyepiece), coupled to a refrigerated DS Qi1-U3 CCD camera (Nikon) with 1,280 × 1,024 resolution (1.5 Mpixels). A DAPI filter cube (excitation filter: 340–380 nm; emission filter: 435–485 nm) was used to detect blue emission. Quantum yield (QY) was measured according to the established procedure using Rhodamine 6G (Sigma, USA) in water at 405 nm (violet laser, 150 mW, Roithner LaserTechnik, GmbH coupled to USB4000 VIS-NIR spectrophotometer, Ocean Optics).

X-ray diffraction (XRD) patterns were recorded using a PANalytical X´Pert diffractometer (Cu-Kα radiation with λ = 1.5406 Å). Measurements were performed in the 2θ range of 15–75º with steps of 0.06º.

Nanostructural characterisations of ZnS QDs, based on images and selected area electron diffraction patterns (SAED), were conducted by transmission electron microscopy (TEM) with a Tecnai G2-20-FEI microscope at an accelerating voltage of 200 kV. Energy-dispersive X-ray spectra (EDX) were collected for chemical analyses. In all TEM analyses, samples were prepared by dropping colloidal dispersions onto a holey carbon grid after the purification procedure developed in this study was performed. QD sizes and distribution data were obtained based on the TEM images by measuring at least 100 randomly selected nanoparticles using an image processing program (ImageJ software, version 1.48; National Institutes of Health).

2.4. Immunohistochemistry assays - fluorescence imaging of lymphoma cells labelled with ZnS immunoconjugates

A human B-cell lymphoma cell line overexpressing the CD20 antigen at the surface (Toledo cells; American Type Culture Collection [ATCC], Manassas, USA, Catalogue No. CRL-2631) was maintained at 37ºC and 5% CO_2. Toledo cells were grown in ATCC-formulated RPMI-1640 Media (Catalogue No. 30-2001), supplemented with foetal bovine serum (FBS; Sigma Aldrich, St Louis, USA) at a final concentration of 10%.

Colloidal suspensions of ZnS QDs at a concentration of approximately 2.0 $\mu mol \cdot L^{-1}$ were used in fluorescence imaging experiments. Toledo cells (3×10^5 $cells \cdot mL^{-1}$) expressing the CD20 antigen were incubated with ZnS_CHI-abCD20 immunoconjugates (1:1) in microfuge tubes for 1 hour at 37ºC. Toledo cells were also incubated with mock ZnS_CHI QDs as a negative control. Toledo cells normally grow in suspension. However, when Toledo cells (500 µL) were mixed with ZnS QDs on a glass microscope slide and centrifuged (800 rpm, 5 minutes) in Universal 320R Centrifuge with 2 mL cyto chambers and chamber cyto slide carriers (Hettich Lab Technology, Kirchlengern, Germany), they adhered to a solid support. ZnS_CHI-abCD20 samples prepared in this manner without Toledo cells were used as blanks. Supernatants were discarded to remove unbound ZnS QDs and the attached (solid-phase) cells were fixed for 30 minutes in 4% paraformaldehyde in phosphate buffered saline (PBS, 1.0 $mg.L^{-1}$). After removing the fixative, ZnS QD immunoconjugates bound to Toledo cells were examined with a Ti-U inverted fluorescence microscope (Nikon; 130 W/Hg lamp, 20× objective, 10× eyepiece, DAPI filter cube) coupled to a refrigerated DS Qi1-U3 CCD camera (Nikon, 1.5 Mpixels). Intensity fluorescence profiles were obtained using NIS-Elements imaging software (Nikon). For each system, 15 measurements were collected under the same conditions (lamp control, exposure time, and auto gain) and averaged.

2.5. Cell viability - non-radioactive cytotoxicity assays

A fibroblast-like cell line from the kidney of a normal adult African green monkey (Vero cells; ATCC Catalogue No. CCL-81) was cultured in Minimum Essential Medium (MEM; Sigma, St Louis, MO, USA) supplemented with 10% heat-inactivated FBS.

Cell viability was tested using the CytoTox®96 Non-radioactive Cytotoxicity Assay (Promega, Madison, WI, USA), according to the manufacturer´s instructions. Vero cells were suspended in MEM supplemented with 10% FBS and plated in a 96-well U-bottom microtiter plate at 1.6×10^4 cells/well. After 24 hours of growth at 37°C in an atmosphere of 5% CO_2, the supernatants were discarded and QD-chitosan conjugates (ZnS_CHI) were added to individual wells in duplicate at increasing concentrations (ranging from 1.0% to 10.0%) in MEM containing 2% FBS. The plate was incubated, and the absorbance of supernatants at 490 nm was recorded to determine the release of lactate dehydrogenase (LDH) after 24 h and 72 h of incubation. The

average absorbance values for the culture medium background and serum (A) was subtracted from experimental LDH release (B) and maximum LDH release (100% cell death; C) values. Percent cell viabilities were calculated using Equations (1) and (2), as follows:

$$\text{Cytotoxicity (\%)} = [(B-A)/(C-A)] \times 100\% \quad \text{(Eq. 1)}$$

$$\text{Cell viability (\%)} = 100\% - \text{Cytotoxicity (\%)} \quad \text{(Eq. 2)}$$

Changes in Vero cell morphology were investigated, following exposure to 1.0%, 5.0%, and 10.0% ZnS-chitosan (ZnS_CHI) bioconjugates in MEM with 2% of FBS. Optical microscopy images of cells were captured using a Ti-U inverted microscope (Nikon; 130 W/Hg lamp, 20× objective, 10× eyepiece) coupled to a cooled DS Qi1-U3 CCD camera (Nikon) with a resolution of 1.5 Mpixels. To validate the importance of using zinc as the metal precursor (Zn^{2+}) for synthesising QDs for nanomedicine applications from a green chemistry perspective, CdS-chitosan (CdS-CHI) conjugates were also evaluated using Vero cells. CdS_CHI conjugates were prepared similarly to the procedure used to generate ZnS_CHI conjugates (described previously), using cadmium perchlorate hydrate ($Cd(ClO_4)_2 \cdot 6H_2O$; Aldrich, USA) dissolved in deionised water (8×10^{-3} mol·L^{-1}) as the metal precursor source. Next, analogous cell viability assay was performed using CdS-CHI conjugates to compare with ZnS-CHI nanoconjugates.

3. RESULTS AND DISCUSSION

3.1. Characterisation of ZnS immunoconjugates

3.1.1. Characterisation of ZnS immunoconjugates by SDS-PAGE

The abCD20 antibody was conjugated to the chitosan using the most common biochemical protocol based on the EDC/sulfo-NHS as highly efficient ‘zero-length’ crosslinking agents. Basically, the reaction mediated by EDC/sulfo-NHS activates the carboxyl groups of the antibodies for linking with the pendant amine groups of chitosan, yielding to chitosan-antibody conjugates bound by stable covalent amide bonds (RC(O)NR’R’’) [31-33].

So, SDS-PAGE analysis was performed to verify the conjugation between chitosan amine groups and the carboxylic-end of anti-C20 antibody (chitosan-abCD20 immunoconjugates). Figure 1A shows the SDS-PAGE results, with reference bands associated with the free antibody (abCD20) showed in lane 3. As expected, after the EDC-mediated crosslinking reaction, no band corresponding to the unbound anti-CD20 antibody (i.e. ‘free’ abCD20) was observed in lane 2, demonstrating that the abCD20 was chemically conjugated to chitosan with high efficiency. In addition, no antibody crosslinking (abCD20-abCD20 species) resulting from side reactions with EDC was detected by SDS-PAGE.

3.1.2. Characterisation of ZnS immunoconjugates by FTIR spectroscopy

FTIR spectroscopy was also performed for a more detailed investigation of the chemical reaction leading to the formation of immunoconjugates. FTIR spectra are presented in Figure 1B with the wavenumber ranging from 1750 to 1500 cm^{-1}, which is the typical region associated with primary amide groups. Because chitosan is a copolymer composed of repeating N-acetyl-D-glucosamine and D-glucosamine units [34], absorption peaks at 1650–1630 cm^{-1}, 1590–1570 cm^{-1}, and 1560–1550 cm^{-1}, assigned to carbonyl stretching of secondary amides (amide I bands), N-H bending vibrations of deacetylated primary amines (-NH_2), and N-H bending vibrations of amide II bands, respectively, were detected with the starting material (Figure 1B(a)). Thus, by comparing the FTIR spectra of CHI (Figure 1B(a)) and ZnS immunoconjugates (Figure 1B(b)), the vibrational band corresponding to primary amine groups (1570–1590 cm^{-1}) is reduced, while the absorption band at 1650–1630 cm^{-1}, associated with the formation of new amide bonds and the major bands of secondary structure of antibodies increased [35-36]. FTIR is widely used as a qualitative spectroscopic method for investigating chemical functionalities in materials, but it may be also utilized for performing semi-quantitative analysis by considering the ratio of absorbance intensities (height or peak areas) [34]. Figure 1C shows the evolution of the amide I (1650 cm^{-1}, baseline 1725–1175 cm^{-1}) and primary amine (1570 cm^{-1}, baseline 1725–1175 cm^{-1}) bands, using the C-O-C stretching band of the saccharide ring at 920 cm^{-1} (baseline 1171–885 cm^{-1}) as the internal reference band. It is noteworthy that the relative absorbance of C=O stretching bands of the QD immunoconjugates (QD_CHI-abCD20) increased, and the relative absorbance of the –NH_2 vibration band caused by the formation of the amide bonds between primary amines from chitosan and carboxylic groups from antibodies decreased.

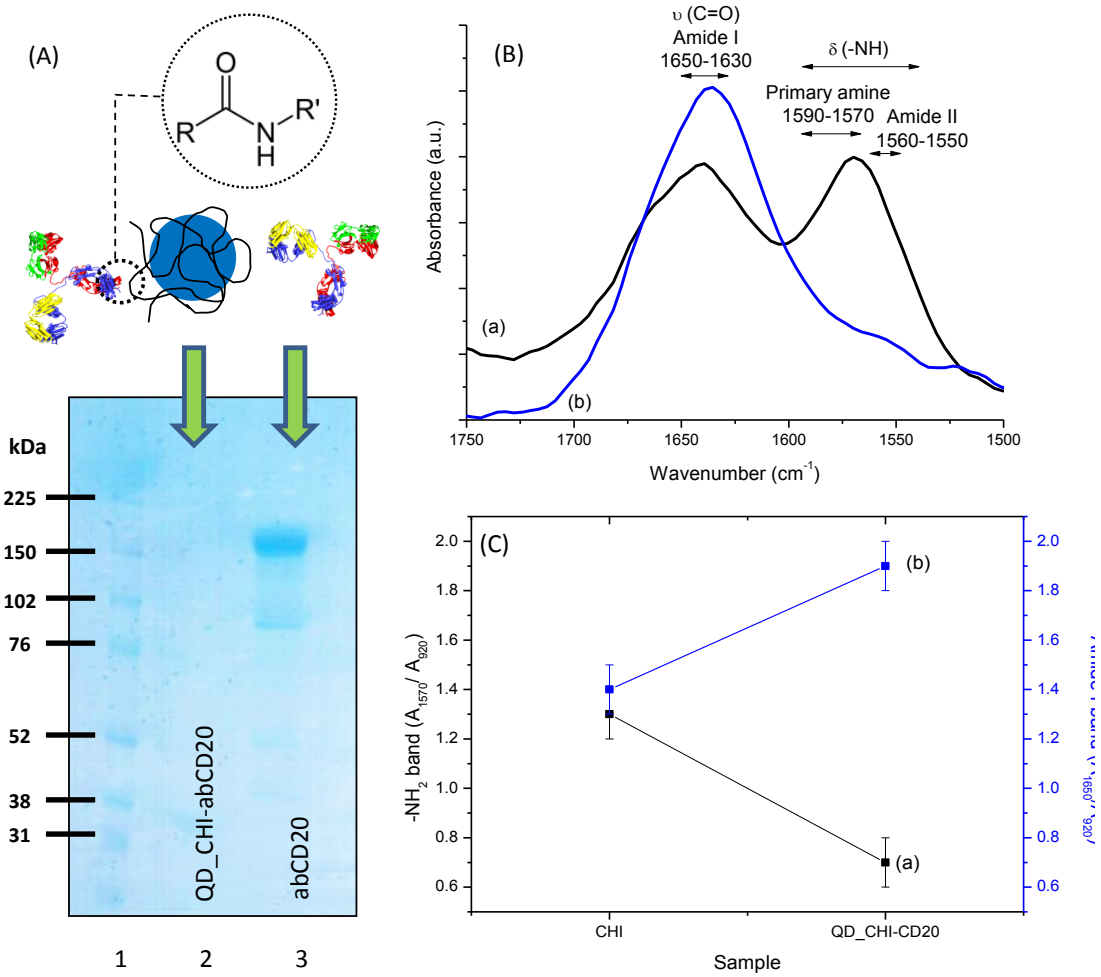

Figure 1. (A) Confirmation of chitosan- antibody conjugation (CHI-abCD20) by SDS-PAGE and Coomassie Brilliant Blue staining. Lane 1, Amersham Full Range Rainbow Recombinant Protein Molecular weight Marker. Lane 2, ZnS nanoconjugates with CHI-abCD20 ligand (absence of bands due to the formation covalent amide bond). Lane 3, abCD20 band at 150 kDa. (B) Infrared spectra of (a) CHI and (b) ZnS_CHI-abCD20. (C) Evolution of primary amine bands (a) and amide I bands (b) due to the EDC-NHS coupling reaction.

3.1.3. Characterisation of ZnS immunoconjugates by UV-Vis spectroscopy

The UV-Vis spectroscopy results with abCD20, ZnS_CHI, and ZnS_CHI-abCD20 immunoconjugates are summarized in Figure 2A and Figure 2B. As the reference, it can be observed in the spectrum of the abCD20 antibody ((abCD20, Figure 2A(a)), an absorption maxima between 275 and 280 nm, which is mostly caused by the electronic transitions π-π^* of cyclic amino acids, such as tryptophan, phenylalanine, and tyrosine present in the protein [32,37]. The spectrum of the colloidal ZnS QDs capped by chitosan (ZnS_CHI, Figure 2A(b)) exhibited a sharp increase in absorbance at approximately 325 nm, followed by a broad

absorption band between 270 and 300 nm. This behaviour was assigned to the nucleation/growth of ZnS nanoparticles within the 'quantum confinement regime' leading to the blue-shift observed in the curves compared to the ZnS bulk value (arrow at λ = 343 nm). Comparing the UV-Vis absorption spectra of ZnS_CHI (Figure 2A(b), without abCD20 conjugation) and the ZnS_CHI-abCD20 antibody conjugates (Figure 2A(c)) suggests that the relative increase in absorption intensity at 275 nm was probably due to the presence of antibody molecules in the conjugates, overlapping the absorption associated with the first excitonic transition of ZnS quantum dots. These findings also confirmed the SDS-PAGE and FTIR results described above indicating that the chitosan-abCD20 antibody bioconjugation occurred.

When considering the application of QD-immunoconjugates as optically active nanoprobes, it is important to properly characterise the band gap transitions and associate them with the properties of the system, based on semiconductor physics and chemistry. Thus, the band gap of quantum dots (E_{QD}) was assessed from absorption coefficient data as a function of wavelength using the 'Tauc relation' (Figure 2B) [38], considering ZnS as a direct band gap semiconductor. This procedure allows the calculation of the dimensions of primary nanoparticles in diluted colloidal suspensions *in situ* after the average size of the ZnS nanocrystals is estimated using an empirical model reported in the literature [39-40], which relates the nanoparticle radius (R) to the optical band gap (E_{QD}) from a UV-Vis spectrum (Equation.3).

$$R(E_{QD}) = [0.32-2.9*(E_{QD}-3.49)^{1/2}] / 2*(3.50-E_{QD}) \quad \text{(Eq. 3)}$$

The optical band gap value (E_{QD}) extracted from the curve using the Tauc relation and the calculated blue-shift ($\Delta E = E_{QD} - E_g$, where E_g is the band gap of 'bulk ZnS' equal to 3.61 eV for ZnS with cubic structure) and diameter (2R) are showed in Figure 2B. These results provide evidence that ZnS QDs were effectively produced in aqueous colloidal media, as the band gap energy values (blue-shift values) of the semiconductors were markedly greater compared to the ZnS bulk. As a consequence, the average ZnS nanocrystal size (2R = 3.6 ± 0.2 nm) is smaller than that of bulk particles (> 6.6 nm).

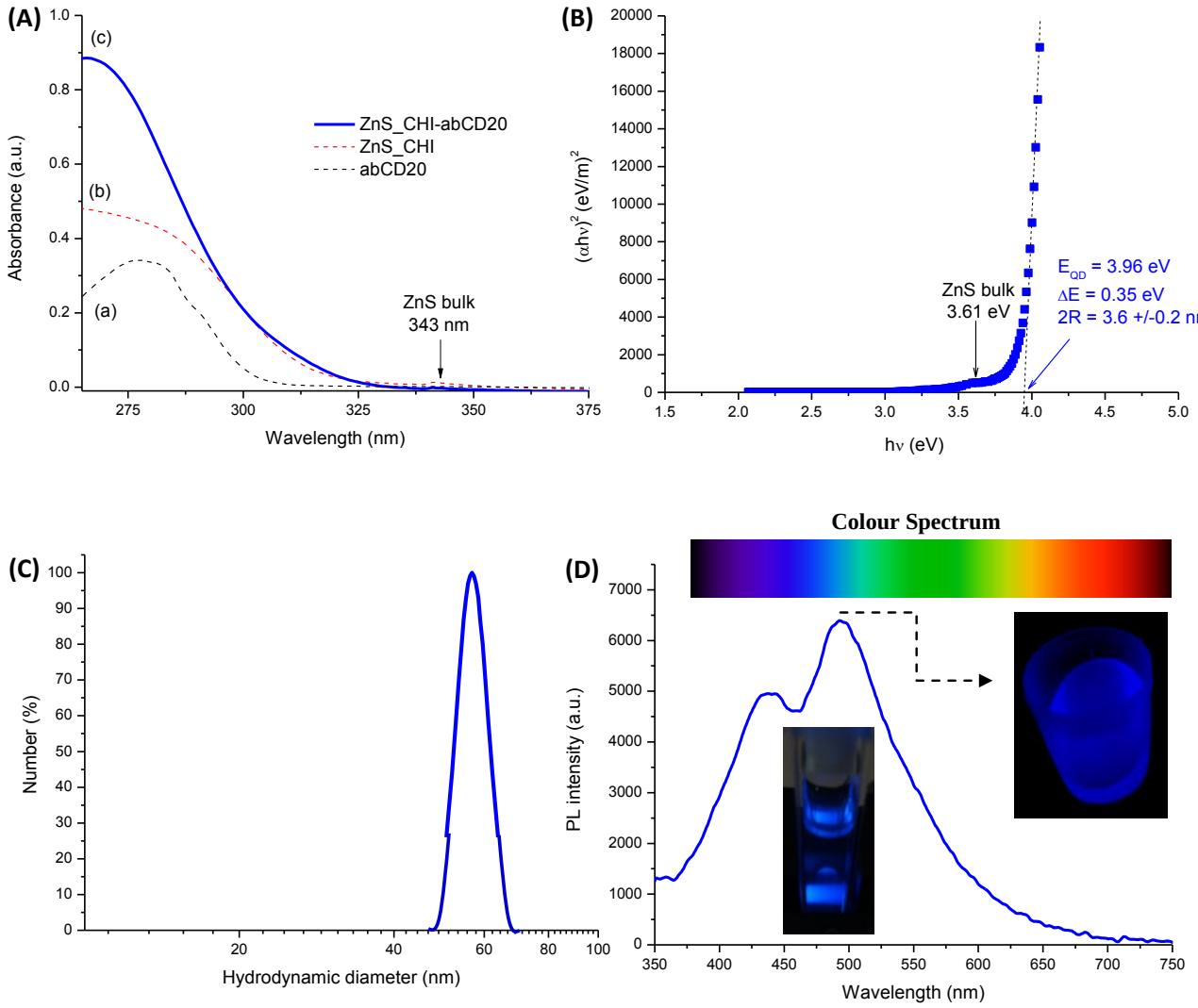

Figure 2. (A) UV-vis spectroscopy analysis of (a) antibody abCD20, (b) ZnS-Chitosan conjugate and (c) ZnS-immunoconjugate. (B) Optical band gap using 'Tauc' relation of ZnS-conjugates. (C) DLS results for ZnS-immunoconjugates aqueous colloidal dispersions. (D) PL spectra of ZnS-QDs immunoconjugates (inset: blue luminescence of ZnS-QDs under UV excitation).

3.1.4. Characterisation of ZnS immunoconjugates by DLS and ZP analyses

In addition to UV-Vis analysis, DLS experiments were performed with aqueous dispersions of ZnS immunoconjugates to determine the nanoparticle hydrodynamic radius (H_R) and the size distribution. For colloidal QDs, the H_R measurement is valuable information for studying the chemical stability and possible interactions with other molecules. Figure 2C shows the average size of ZnS_CHI-abCD20 conjugates of 56.9 ± 0.8 nm, which is much larger than the estimated size from UV-Vis spectroscopy. This value corresponds to the hydrodynamic diameter (H_D), which is different from the primary semiconductor nanoparticle size calculated from UV-Vis

absorbance curves (~3.6 nm). The DLS results are explained by considering the contributions of the ZnS inorganic core and chitosan-antibody organic shell, including the influence of solvation layers, excluded volume interactions, polyelectrolyte effects, and constraints in bond and rotation angles [32, 41]. The polydispersity index of prepared ZnS immunoconjugates size distribution was 0.005, indicating that the size distribution is relatively narrow. Thus, DLS offers complementary information regarding the the overvall dimensions of colloidal immunoconjugates, which is of paramount importance for applications in nanomedicine.

The ZP measurement of ZnS immunoconjugates at pH 6.0 ± 0.1 was +24.7 ± 2.1 mV. This value indicated that the ZP was predominantly influenced by surface charges of the antibody as the ZP of chitosan approaches zero at pH values around pH 6.0 (pKa ~6.5). The isoelectric point of antibodies is above this pH, typically close to 7.0. In addition, as the ZP result was below +30 mV, ZnS immunoconjugates were not predominantly electrostatically stabilised, but relied on the steric hindrance of the polymer-antibody shell to prevent close contact between the nanoparticles [42].

3.1.5. Characterisation of ZnS immunoconjugates by photoluminescence spectroscopy.

In order to be used as biomarker for cancer detection, the fluorescent behaviour of the ZnS immunoconjugates is crucial. Figure 2D shows the photoluminescence (PL) spectra collected at RT of the ZnS QD nanoconjugates. The band edge (excitonic) emission of ZnS was not detected and the typical emission peaks in the range of wavelength from 400 to 500 nm (violet-blue) were observed [43]. According to the energy levels diagrams reported by Wageh and co-worker [44] and Becker *et. al.* [45], the high-energy emission bands (wavelengths below 450 nm) observed in the PL spectra were mostly associated with V_s (vacancies of sulphur, S^{2-}) and I_{Zn} (Zn^{2+} at interstitial sites at the nanocrystal lattice) defects. Such PL behaviour can be associated with the fact that the ZnS QDs were produced using a 2:1 cation:anion molar ratio, i.e. an excess of metal cations (Zn^{2+}) compared to anions (S^{2-}), selected for favouring their stabilisation during the synthesis by chemical interactions at the surfaces with chitosan ligands (amine and hydroxyl groups). On the other hand, it may have also contributed to the incorporation of Zn^{2+} into the lattices at interstitial sites. The other emission band in the PL spectrum centred at approximately 470 nm may be assigned to surface defects [44]. Additionally, the quantum yield (QY) of the ZnS QD nanoconjugates produced in this study was approximately 5.0%, which is in good agreement with the literature of ultra-small quantum dots synthesised by aqueous colloidal route at low temperatures (typically QY=1% to 20%) [12].

3.1.6. Characterisation of ZnS immunoconjugates by morphological and structural analysis

In this study, the morphological and structural features of ZnS quantum dots were characterised by transmission electron microscopy (TEM) coupled to an energy dispersive X-ray (EDX) microprobe and selected area electron diffraction (SAED) analysis. In addition, XRD was used to investigate the crystal structure of the semiconductor nanoparticles produced. Figure 3A shows a representative sample of ZnS stabilized with chitosan-antibody in sphere-shaped nanoparticles. The size distribution histogram (Figure 3B) presented fairly monodispersed nanoparticles with the average size of 3.8±0.4 nm in good agreement with the values obtained from the UV-Vis optical absorbance (3.6±0.2 nm) in previous section. EDX spectra (Figure 3C) showed the chemical analysis of nanocrystals with Zn and S as the major elements, excluding the copper, oxygen and carbon peaks related to the TEM grid and the polymer stabiliser. The XRD pattern of ZnS QD immunoconjugates presented 3 major peaks centred at $2\theta \sim 28.7^{o}$, ~ 48.0^{o} and ~56.3^{o} that could be assigned to the planes (111), (220), and (311) of ZnS of cubic lattice structure (zinc blend also referred to as sphalerite, JCPDS 05-0566). These results were compatible with the lattice fringes of an interplanar distance of approximately 0.32 ± 0.02 nm, assigned to the (111) plane and revealed by the SAED pattern. Some peak broadening was observed in XRD patterns, which relates to the formation of ultra-small nanocrystals, i.e. ZnS quantum dots [46].

3.2. Immunohistochemistry assays - fluorescence imaging of lymphoma cells labelled with ZnS immunoconjugates

Cancer immunochemistry and immunotherapy tools use immune-affinity properties to detect, target, and treat cancer. These approaches exploit the fact that cancer cells frequently express slightly different molecules on their membranes that can be detected by immune-specific systems. These molecules, known as cancer antigens, are most commonly proteins and peptides. CD20 is a specific transmembrane antigen receptor that is overexpressed in non-Hodgkin lymphoma (NHL) [11, 47]. Thus, Toledo cells (a lymphoma B-cell line) were selected for *in vitro* cellular uptake assays. Figure 4A shows a bright-field phase image of lymphoma cells with typical morphology [11, 47]. Figure 4B shows the fluorescence image obtained from blank (Toledo cells without the ZnS QD fluorophore). The detected background emission is denoted as auto-fluorescence and arises from endogeneous fluorophores when cells are excited by UV-Vis radiation. Considering the emission range of DAPI cube filters, this emission could be associated with pyridine nucleotides [48].

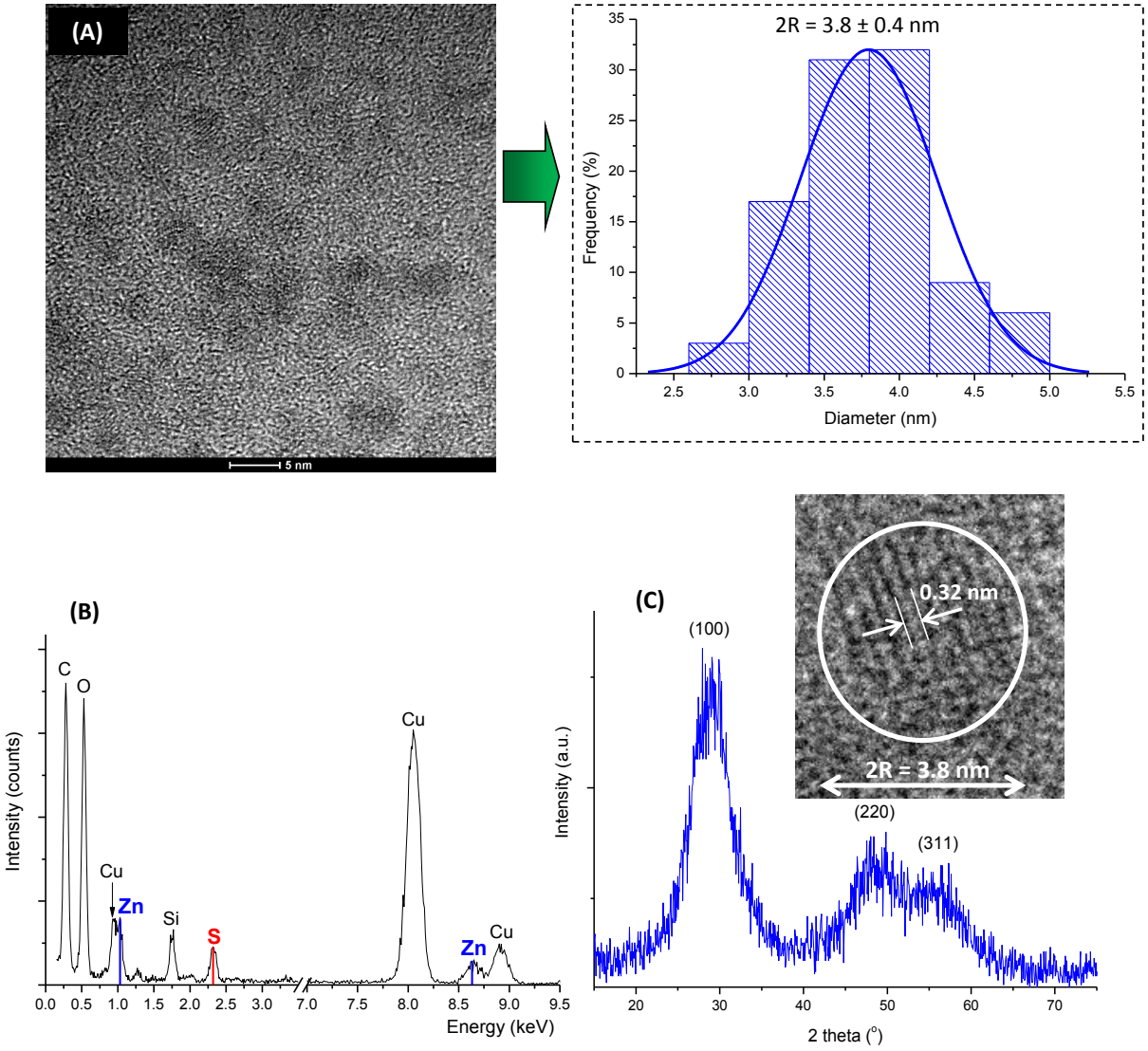

Figure 3. (A) TEM image (left) and particle size distribution histogram of ZnS-QDs bioconjugates (right); (B) EDX spectrum; (C) XRD pattern of ZnS immunoconjugates and the planes of ZnS nanocrystal (inset: SAED nanocrystal lattice spacing image).

Figure 4F indicates the blue fluorescence of B-cell cancer biomarker CD20 (ZnS_CHI-abCD20) in the tested cell line. The fluorescence microscopy image indicated that the tumour cells were specifically labelled by the ZnS QDs conjugated with anti-CD20 antibodies. The maximum fluorescence intensity was observed at the cell membrane because CD20 is a transmembrane protein with the binding site for abCD20 occurring on the cytoplasmic side of cell [11,47]. Negative-control samples (Toledo cells treated with ZnS_CHI, without the abCD20 antibody) showed only minor and unspecific fluorescence (Figure 4D). Quantitative measurements of fluorescence intensity at the cell membranes (Figures 4C, 4E, and 4G related to blank, negative control, and immunoconjugates, respectively) are showed in fluorescent intensity distribution histograms. The fluorescence intensity of ZnS-immunoconjugated nanoparticles (ZnS_CHI-

abCD20) was >200% higher than that observed for samples without conjugated antibodies (ZnS_CHI, negative control) or auto-fluorescence (blank) values. The fluorescent intensity distribution (calculated as the square of the standard deviation/mean intensity) was below 0.005 for all systems. As negative controls, parallel assays were performed with CD20 negative cells, using Vero fibroblast-like cells and the HeLa tumour cell lines, and no fluorescence was detected (data not showed). In summary, these results confirmed that the novel ZnS-immunoconjugates developed in this study were specific and selective towards NHL cancer cells.

3.3. *In Vitro* Cell toxicity assays

Cell-based assays are often used for screening collections of compounds to determine if the test molecules have effects on cell proliferation or show direct cytotoxic effects that eventually lead to cell death. While the major goal of this study was to develop a fluorescent immunoassay for detection NHL cancer cells *in vitro*, cell viability assays were performed with Vero cells as a preliminary evaluation of the cytotoxicity of QD-conjugated nanoparticles for possible future *in vivo* application. Furthermore, as a proof-of-concept, these assays would provide some important information regarding to the relative cytocompatibility or non-toxicity between the novel ZnS bioconjugates compared to the analogous QD-conjugates made with CdS nanocrystals as the inorganic core. Thus, cytotoxicity experiments were performed, based on the absorbance of supernatants from each sample of QD bioconjugates at $\lambda = 490$ nm to determine the release of lactate dehydrogenase (LDH; Non-Radioactive Cytotoxicity Assay CytoTox® 96 Kit) by the Vero cells.

This assay quantitatively measures LDH, a stable cytosolic enzyme that is released upon cell lysis [49]. The amount of colour formed is proportional to the number of lysed cells. The cell viability was calculated by assuming 100% viability for control cells. The LDH cell viability results of Vero cells after 24 h incubation are summarized in Figures 5A and 5B, for ZnS conjugates and CdS conjugates, respectively. It can be clearly observed a significant difference on the cell viability results by comparing the ZnS-based conjugates with the CdS conjugates. At first, ZnS conjugates at all tested concentrations have presented excellent cell viability responses of practically 100% (within the statistical variation). On the contrary, despite the CdS conjugates did not show relevant toxicity at the lowest concentration (1.0%), they have presented much lower cell viability values at higher concentrations, 5.0% and 10%, with approximately 30% and 35% cell death, respectively.

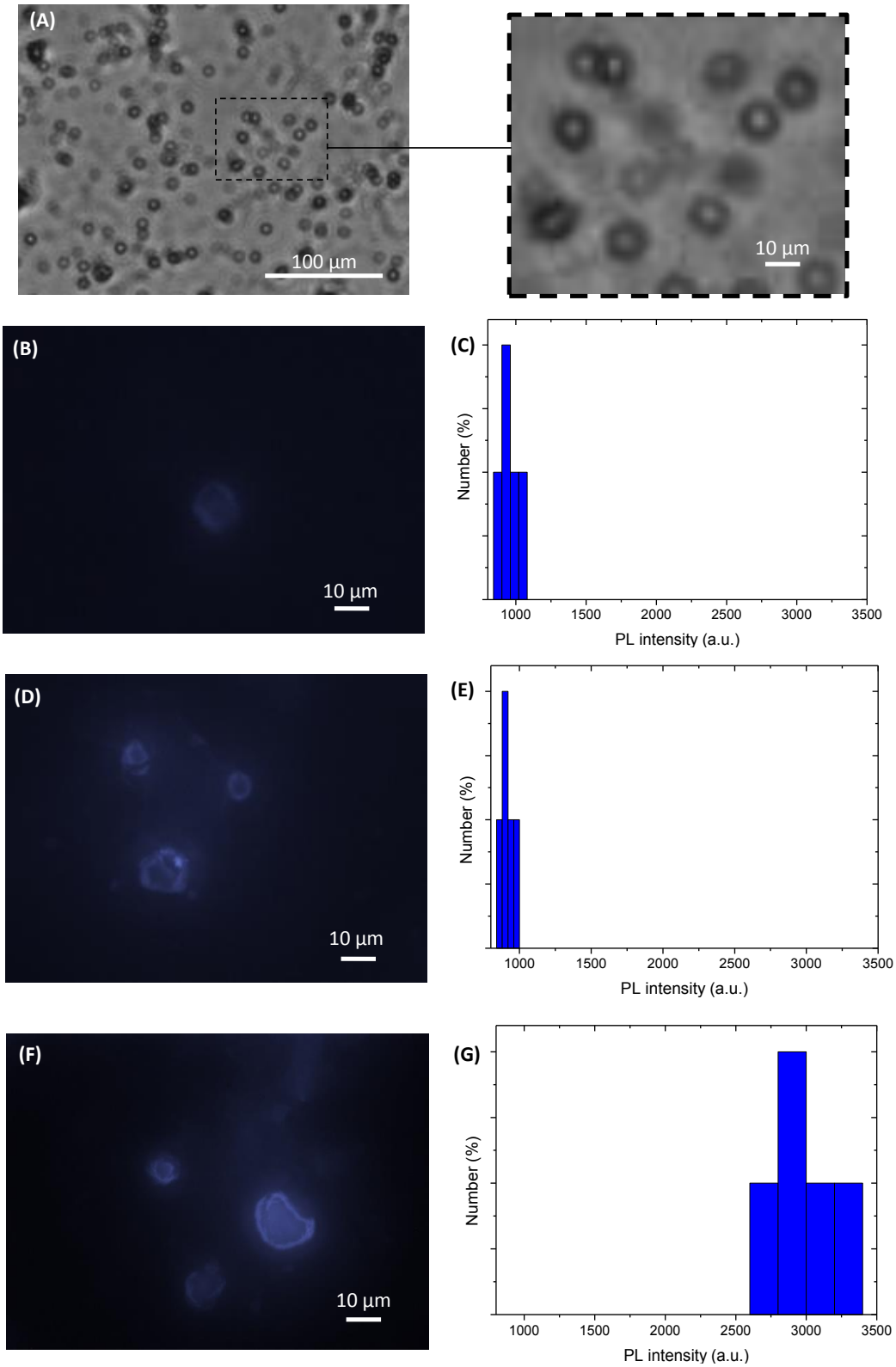

Figure 4. Detection of the B-cell cancer biomarker CD20 internalization through immunofluorescence: Bright-field Microscopy (A). 'Blue' fluorescence images of blank ((B), lymphoma cell without QDs), negative control ((D), lymphoma cells with ZnS_CHI), and immunoconjugates ((F), lymphoma cells with ZnS_CHI-abCD20). Fluorescence intensity profiles of blank (C), negative control (E), and ZnS immunoconjugates (G).

Additionally, bright-field phase images collected by optical microscopy of Vero cells incubated for 24 h with both ZnS and CdS conjugates are presented in Fig. 5(C) and Fig. 5(D) respectively. It may be observed on both images the typical morphological aspects of a fibroblast-like cell line (Vero). However, a striking difference is verified on the ZnS conjugates (Fig.5D) forming a uniform cell monolayer covering the entire bottom of the plate as compared to the CdS sample with several uncoated areas producing a heterogeneous layer.

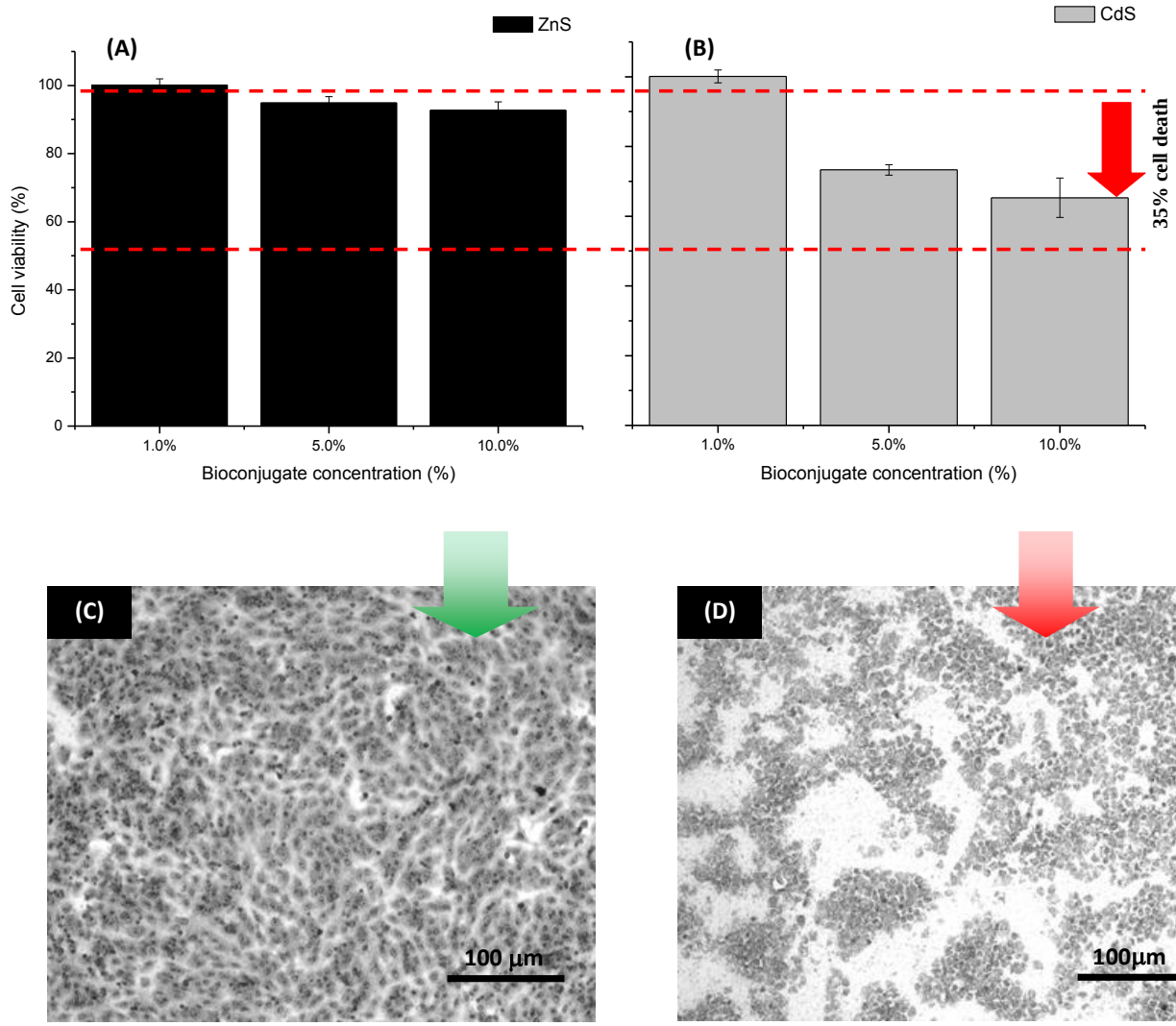

Figure 5. Histograms of Vero cell viability after 24 h exposure at 3 concentrations (1.0%, 5.0%, 10.0%) to ZnS-chitosan (A) and CdS-chitosan (B) conjugates. Bright-field phase images collected by optical microscopy of Vero cell incubated for 24 h with ZnS-chitosan (C) and CdS-chitosan (D) conjugates.

It should be emphasised that these results are very important as far as the initial evaluation of toxicity of the QD nanoconjugates is concerned, which proved the original hypothesis of this research that ZnS bioconjugates are non-cytotoxic, biocompatible, and eco-friendly. On the

other hand, the cadmium-based conjugates demonstrated much lower cell viability towards fibroblast-like cells at higher concentrations (5% and 10%). However, it cannot be affirmed conclusively that CdS nanoconjugates are cytotoxic because there are no absolute or threshold values for cell viability response, but only a relative comparison with ZnS conjugates based on the LDH assay. That is of paramount importance considering the potential biological, pharmaceutical, and medical applicability of these QDs for the future *in vivo* and clinical purposes. As a broad and intricate theme, the toxicity of nanomaterials such as QD conjugates is very controversial and far from being completely understood [17], where undoubtedly several future studies will need to be conducted. Nonetheless, this research pioneered showed that nanomedicine and environmental nanoscience can be gathered for fighting cancer, which is one of the most devastating diseases of the current millennium.

4. CONCLUSIONS

In this study, ZnS QDs surface biofunctionalised by chitosan-antibody immunoconjugates were synthesised at room temperature using a one-pot process in aqueous medium according to an aqueous colloidal chemistry approach. The results demonstrated that the conjugation between the chitosan (CHI) and antibody (abCD20) was made by amide covalent bonds of amine and carboxyl groups, respectively. These immunoconjugates effectively stabilised the formation of ultra-small ZnS nanocrystals with average size of 3.7 nm, predominantly by the interaction of the electron-donors functional groups of chitosan, such as amines and hydroxyls, with Zn^{2+} at the surface of QDs. In addition, they presented blue luminescent behaviour and were active for specific targeting, labelling and bioimaging lymphocyte-B tumour cells based on the affinity between the antibody of the immunoconjugates and the antigen CD20 at the cell membrane. Moreover, the results of the LDH-based cytotoxicity *in vitro* assay using fibroblast-like cell line evidenced that the ZnS-nanoconjugates were cytocompatible, as well as they presented the best cell viability response after 24 and 72 h, in comparison with the analogous CdS-based conjugates. Thus, novel heavy metal-free water-soluble ZnS-immunoconjugate fluorophores were successfully produced using environmentally-friendly chemistry which may be potentially used in the future as nanoprobes in a large number of applications in oncology diagnosis and nanomedicine.

Acknowledgments

The authors acknowledge the financial support from Brazilian Research Agencies CAPES, FAPEMIG, CNPq and FINEP. The authors express their gratitude to the staff at the Microscopy Centre/UFMG for TEM analysis.

Competing interests

The authors declare that they have no competing interests.

References

1. R. P. Feynman, *Engineering and Science,* 1960, **23**:22.
2. C. P. Toumey, *Research in Philosophy and Technology*, 2008, **12**,133.
3. D. F. Emerich, *Expert Opinion on Biological Therapy*, 2005, **5**,1.
4. M. L. Etheridge, S. A. Campbell, Erdman, A. G. Haynes CL, S. M. Wolf, J. Cullough, *Nanomedicine: Nanotechnology, Biology and Medicine*, 2013, **9**,1.
5. W. B. Tan, N. Huang, Y. Zhang, *J. Colloid Interface Sci.,* 2007, **310**,464.
6. H. S. Mansur, A. A. P. Mansur, F. P. Ramanery, F. G. L. M. Borsagli, *Journal of Nanoparticle Research*, 2014, **16**, 1.
7. H. S. Mansur, A. A. P. Mansur, E. Curti, M. V. de Almeida, *J. Mater. Chem. B*, 2013, **1**, 1696.
8. Ferrari, M., *Nat. Rev. Cancer*, 2005, **5**, 161.
9. X. Ma, Y. Zhao, X.-J. Liang , *Acc. Chem. Res.*, 2011, **44**, 1114.
10. H. S. Mansur, A. A. P. Mansur, In *Encyclopedia of Biomedical Polymers and Polymeric Biomaterials*; Mishra, M, Ed.; CRC Press, 2014; *in press*.
11. A. A. P. Mansur, H. S. Mansur, A. Soriano, Z. I. P. Lobato, *ACS Appl. Mater. Interfaces*, 2014, **6** (14),11403.
12. H. S. Mansur, *Wiley Int. Rev. Nanomed. Nanobiotechnol.*, 2010, **2**, 113.
13. H. Wang, T. Wang, X. Wang, R. Liu, B. Wang, H. Wang, Y. Xu Y, J. Zhang, J. Duan, *J Mater Chem.*, 2012, **22**,12532.
14. X. Wang, H. Zhu, Y. Xu, H. Wang, Y. Tao, S. Hark, X. Xiao, Q. Li, *ACS Nano*, 2010, **22**,3302.
15. M. Fang, C. W. Peng, D. W. Pang, Y. Li, *Cancer Biol. Med.* 2012, **9**, 151.
16. M. Green, J. Mater. Chem., 2010, **20**,5797.
17. K-T. Yong, W-C. Law, R. Hu, L. Ye, L. Liu, M.T. Swihart, P.N. Prasad, *Chem. Soc. Rev.*, 2013, **42**,1236.
18. C. L. Salgado, A. A. P. Mansur, H. S. Mansur, F. Monteiro, *RSC Advances*, 2014, **4**, 49016.
19. F. P. Ramanery, A. A. P. Mansur, H. S. Mansur, *Nanoscale Res Lett.*, 2013,**8**(1),512.
20. W. B. Tan, N. Huang, Y. Zhang, *J. Colloid Interface Sci.*, 2007, **310**, 464.
21. H. S. Mansur, A. A. P. Mansur, E. Curti, M. V. de Almeida, *Carbohydr. Polym.*, 2012, **90**, 189.

22. S. Mukherjee, V. Sushma, S. Patra, A. K. Barui, M. P. Bhadra, B. Sreedhar, C. R. Patra, *Nanotechnology*, 2012, **23**,455103.

23. C. Buzea, I. I. Pacheco, K. Robbie, *Biointerphases*, 2007, **2**(4), MR17.

24. A. A. Matthew, W. E. Cameron, C. L. Raston, *Green Chem.*, 2006, **8**, 417.

25. N. Pradhan, X. Peng, *J. Am. Chem. Soc.*, 2007, **129**, 3339.

26. D.Deng, J. Cao, L.Qu, S. Achilefu, Y. Gu, *Phys. Chem. Chem. Phys.*,2013, **15**, 5078.

27. A. Punnoose, K. Dodge, J. W. Rasmussen, J. Chess, D. Wingett, C. Anders, *ACS Sustainable Chem. Eng.*, 2014, **2**(7), 1666.

28. S. K. Mehta, S. Kumar, M. Gradzielski, *J. Colloid Interface Sci.*, 2011, **360**,497.

29. S. A. Cumberland, J. R. Lead, *ACS Sustainable Chem. Eng.*, 2013, **1**(7), 817.

30. A. V. Delgado,F. González-Caballero, R. J. Hunter, L. K. Koopal, J. Lyklema, *Pure Appl. Chem.*, 2005, **77**,1753.

31. C.K.Dixit, S.K. Vashist, B.D. MacCraith, R. O'Kennedy, *Nat. Protoc.* 2011, **6**, 439.

32. H. S. Mansur, A. A. P. Mansur and J. C. González, *Polymer*, 2011, **52**, 1045.

33. G. T. Hermanson, Bioconjugate Techniques, 2nd ed; Elsevier Inc.: Amsterdam, 2008.

34. J. C. C. Santos, A. A. P. Mansur, H. S. Mansur, *Molecules* (Basel. Online), 2013, **18**, 6550.

35. Shire, S.J., Gombotz, W., Current Trends in Monoclonal Antibody Development and Manufacturing, K. Bechtold-Peters, J. Andya (Eds.), 2010, XIV, 354 p.

36. H. S. Mansur, A. A. P. Mansur, *J. Mater. Chem.*, 2012, **22**, 9006.

37. A. A. P. Mansur, H. S. Mansur, J. González, *Sensors*, 2011, **11**(10), 9951.

38. J. Tauc J, A. Menth, *J. Non-Cryst Solids*, 1972, **8–10**,569.

39. A. Jaiswal, P. Sanpui, A. Chattopadhyay, S. S. Ghosh, Plasmonics 2011, **6**,125.

40. M. Mall, L. Kumar, *J. Lumin.*, 2010, **130**,660.

41. T. Pons, H. T. Uyeda, I. L. Medintz, H. Mattoussi, J. *Phys. Chem. B*, 2006, **220**, 20308.

42. A. A. P. Mansur, J. B. Saliba, H. S. Mansur, *Colloids Surf.-B*, 2013, **111**, 60.

43. R. Chen, D. Li, B. Liu, Z. Peng, G. G. Gurzadyan, O. Xiong, H. Sun, *Nano Lett.*, 2010, **10**,4956.

44. S. Wageh, Z. S. Ling, X . Xu-Rong, *J. Cryst. Growth*, 2003, **255**, 332.

45. W. G. Becker, A. J. Bard, *J. Phys. Chem.*, 1983, **87**,4888.

46. K. Tarasov, D. Houssein, M. Destarac, N. Marcotte, C. Gérardi, D. Tichit, *New J. Chem.*, 2013, **37**, 508.

47. D. G. Maloney, *N. Engl. J. Med.*, 2012, **366**, 2008.

48. M. Monici, *Biotechnol. Annu. Rev.*, 2005,**11**, 227.

49. J. M. Hernández, M. H. Bui, K. R. Han, H. Mukouyama, D. G. Freitas, D. Nguyen, R. Caliliw, P. I. Shintaku, S. H. Paik, C. L. Tso, R. A. Figlin, A. S. Belldegrun, *Clin. Cancer Res.*, 2003, **9**, 1906.

Table of Contents

Graphical Abstract

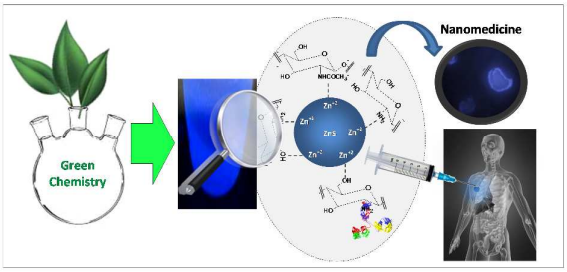

Novelty

Nanomedicine meets green chemistry: Biocompatible ZnS-immunoconjugates were developed to detect *in vitro* NHL cancer cells using an environmentally-friendly aqueous process.